JOURNAL OF MATERIALS SCIENCE 20 (1985) 3881–3889

Non-isothermal calorimetric determination of precipitate interfacial energies

ARI VARSCHAVSKY
Universidad de Chile, Facultad de Ciencias Físicas y Matemáticas, Instituto de Investigaciones y Ensayes de Materiales (IDIEM), Casilla 1420, Santiago, Chile

Equations suitable for computing specific interfacial energies of precipitates dissolving by a first order transformation were developed on the basis of the singularities taking place at the critical temperature, T_c, under equilibrium conditions. These equations employ data which can be determined by differential scanning calorimetry. Also the conditions for reaching dynamic equilibrium of particle volume fraction below T_c are analysed in terms of a maximum permissible experimental heating rate. The results obtained for disperse order in αCu–Al alloys are in good agreement with those expected from the observed particle features.

1. Introduction

The physical characteristics of solid state interfaces play an important role in many aspects of materials behaviour [1]. One of the major parameters which enable one to evaluate quantitatively these characteristics is the specific interfacial energy, σ, which is fundamental to theories of recrystallization, grain growth, fracture, precipitate nucleation and growth and strength of dispersed phase alloys. Most of direct and indirect techniques developed for measuring σ are concerned with boundaries in single phase materials [2] (e.g. grain or twin boundaries), instead there has been little progress in obtaining absolute values of σ in a multiphase material particularly when one phase is finely dispersed in the other.

Two major papers exist in the literature employing calorimetric methods: in one, σ was calculated from solution calorimetry of alloys containing varying dispersions (and hence varying interfacial areas) of two phases [3]; in the other σ was calculated from isothermal calorimetry by measuring the heat evolution during precipitate coarsening [4].

The purpose of the present contribution is to develop expressions suitable to compute σ for precipitates which undergo a first order transition during dissolution by employing data obtained from non-isothermal differential scanning calorimetry (DSC). These expressions are tested in the determination of the specific interfacial free energy of Cu_3Al ordered domains in αCu–Al alloys which are a good example of a stable heterogeneous microstructure [5–7].

2. Theoretical considerations

2.1. Evaluation of σ

The method presented here for calculating precipitate interfacial energies utilizes as primary inputs the Gibbs–Thomson and mass conservation equations, together with the singularities occurring at the critical temperature during particle dissolution by a first order transformation.

The generalized Gibbs–Thomson equation for the variation of solubility with particle size can be written as [8]:

$$c_M - c_0 \exp\left(\frac{4V_m\sigma}{RTD}\right) = F(c_M, D, T) \equiv 0 \quad (1)$$

where c_M is the equilibrium solubility adjacent to a particle of diameter D, c_0 is the equilibrium

0022–2461/85 $03.00 + .12

solubility adjacent to an infinitely large particle, V_m is the molar volume of the precipitate phase, R is the universal gas constant and T the absolute temperature. $F(c_M, D, T)$ is an implicit function of c_M, D and T. If spherical precipitates are considered, the actual volume fraction, V, as a function of the extended volume fraction, V_{ex}, is given by [9]:

$$V = 1 - \exp(-V_{ex}) \quad (2)$$

V_{ex} is the volume fraction that would exist if there were no impingement and it is related to the precipitate number per unit volume, N (considered unchanged up to the critical temperature T_c) by the expression:

$$V_{ex} = \frac{\pi}{6} ND^3 \quad (3)$$

Since the concentration rise at the precipitate surface is quite small [10], the required balance of material can be set as:

$$V = \frac{\bar{c} - c_M}{c_p - c_M} \quad (4)$$

where c_p and $\bar{c}$ are the particle and alloy compositions respectively. Then, from Equations 2, 3 and 4:

$$1 - \exp\left(-\frac{\pi}{6} ND^3\right) - \frac{\bar{c} - c_M}{c_p - c_M} = G(c_M, D) \equiv 0 \quad (5)$$

where $G(c_M, D)$ is an implicit function of c_M and D. With Equations 1 and 5, we are interested in determining the temperature dependence of the rate of variation of c_M and D with T under equilibrium conditions, particularly at T_c where $\partial c_M/\partial T$ and $\partial D/\partial T$ change abruptly since $V = V_c$ for $T = T_c^-$ and $V = 0$ for T_c^+, V_c being the critical volume fraction (i.e. at the onset of precipitate dissolution). The computational details are given in the Appendix. Solving simultaneously the equations $dF = 0$ and $dG = 0$, after taking T as the independent variable, we find:

$$\frac{\partial c_m}{\partial T} = -\left(\frac{\partial F}{\partial T}\frac{\partial G}{\partial D}\right) J^{-1} \quad (6)$$

and

$$\frac{\partial D}{\partial T} = \left(\frac{\partial F}{\partial T}\frac{\partial G}{\partial c_M}\right) J^{-1} \quad (7)$$

where J is the Jacobian of F and G with respect to c_M and can be expressed as:

$$J = \frac{\partial F}{\partial c_M}\frac{\partial G}{\partial D} - \frac{\partial F}{\partial D}\frac{\partial G}{\partial c_M} \quad (8)$$

The condition of discontinuity of the left-hand side terms for the partial derivatives of Equations 6 and 7 at $T = T_c^-$ requires $J = 0$. At this temperature:

$$\left.\begin{aligned} D &= D_c \\ c_M^c &= \frac{\bar{c} - V_c c_p}{1 - V_c} \\ V_c &= 1 - \exp\left(-\frac{\pi}{6} ND_c^3\right) \end{aligned}\right\} \quad (9)$$

where D_c is the critical diameter and c_M^c the critical equilibrium solubility adjacent to a particle of diameter D_c and V_c the critical volume fraction. Since:

$$\left.\begin{aligned} \frac{\partial F}{\partial c_M} &= 1, \quad \frac{\partial F}{\partial D} = \frac{4c_0 V_m}{RTD^2}\exp\left(\frac{4V_m\sigma}{RTD}\right) \\ \frac{\partial G}{\partial c_M} &= \frac{c_p - \bar{c}}{(c_p - c_M)^2}, \quad \frac{\partial G}{\partial D} = \frac{\pi}{2} ND^2 \\ &\quad \times \exp\left(-\frac{\pi}{6} ND^3\right) \end{aligned}\right\} \quad (10)$$

and considering that

$$V_{ex}^c = \ln\frac{1}{1 - V_c},$$

after substituting Equations 9 and 10 into Equation 8, the specific interfacial energy yields:

$$\sigma = \frac{3RT_cD_c}{4V_m}\frac{(c_p - \bar{c})}{(\bar{c} - V_c c_p)}\ln\left(\frac{1}{1 - V_c}\right) \quad (11)$$

Alternatively, Equations 1 and 5 can be written as:

$$T = T(D, c_M), \qquad c_M = c_M(D, N) \quad (12)$$

It can also be demonstrated that:

$$\left(\frac{\partial T}{\partial D}\right)_N = \left(\frac{\partial T}{\partial D}\right)_{c_M} + \left(\frac{\partial T}{\partial c_M}\right)_D \left(\frac{\partial c_M}{\partial D}\right)_N, \quad (13)$$

then from Equations 1 and 5 in the form of Equations 12 and from Equation 13, after imposing the required condition $(\partial T/\partial D)_N = 0$ for $T = T_c^-$, Equation 11 can readily be obtained. If $V_c \ll 1$, that is if impingement is negligible, $\ln[1/(1 - V_c)] \simeq \ln(1 + V_c) \simeq V_c$,

hence Equation 11 becomes:

$$\sigma_f = \frac{3RT_cD_cV_c}{4V_m}\frac{(c_p - \bar{c})}{(\bar{c} - V_c c_p)} \quad (14)$$

where σ_f relates to the actual specific surface energy by:

$$\sigma = \sigma_f \frac{1}{V_c}\ln\left(\frac{1}{1 - V_c}\right) \quad (15)$$

In order to evaluate σ, Equation 11 requires the knowledge of T_c, D_c and V_c, which can be determined making use of differential scanning calorimetric (DSC) experiments.

Generally D_0, the average particle diameter at room temperature corresponding to a volume fraction V_0, is available in the literature. If ΔH_c is the enthalpy associated with the dissolution of particles at a low heating rate (where dynamic equilibrium prevails below T_c) and ΔH_0 is the enthalpy associated with particle dissolution at high heating rate (when for kinetic reasons an off equilibrium volume fraction retained from room temperature dissolves), one has:

$$V_c = \left(\frac{\Delta H_c}{\Delta H_0}\right) V_0 \quad (16)$$

If impingement is considered, the critical precipitate diameter can be written as:

$$D_c = \left(\frac{6}{\pi N} \times \ln\left\{\frac{1}{\left[\frac{\Delta H_0}{\Delta H_c} + \exp\left(-\frac{\pi}{6}ND_0^3\right) - 1\right]\frac{\Delta H_c}{\Delta H_0}}\right\}\right)^{1/3} \quad (17)$$

Equation 17 needs the knowledge of N, which is not usually available. As a first approximation it can be set

$$D_c = \left(\frac{\Delta H_c}{\Delta H_0}\right)^{1/3} D_0, \quad (18)$$

furthermore if $\Delta H_c \simeq \Delta H_0$, $D_c = D_0$ can be used. The value of V_c can be determined from ΔH_c and the molar heat of dissolution of the precipitates, ΔH_p. In fact,

$$V_c = \frac{K}{\Delta H_p}\Delta H_c \quad (19)$$

where $k = (MW)_p(\varrho_s/\varrho_p)$, $(MW)_p$ being the molecular weight of the precipitate and ϱ_s and ϱ_p, the alloy and precipitate density respectively. Alternatively, if ΔH_p is unknown, but if N and D_0 are available, V_c can be obtained from Equation 16. Finally, T_c is determined as the onset temperature at which the DSC trace leaves the base line.

2.2. The rate of equilibration below T_c

The accuracy of the determination of σ is conditioned to the fact that the system equilibrates during the constant heating rate experiment before T_c is reached. This requirement determines a maximum heating rate, α_m, that can be employed. An estimation of α_m is given below.

When the temperature is rapidly raised (or lowered) the alloy cannot reach momentarily the equilibrium state for the temperature change, because atomic rearrangements for the change need a certain time. The rate of approach to the equilibrium state has been treated theoretically by Bragg and Williams [11]. They have considered an alloy at a temperature T whose degree of order (particle volume fraction in the present study) is different from that corresponding to the dynamic equilibrium at that temperature and corresponds to the equilibrium degree of order at a different temperature θ. They assumed that the rate of approach to equilibrium is given by:

$$\frac{d\theta}{dt} = -\left(\frac{\theta - T}{\tau}\right) \quad (20)$$

where τ, the time of relaxation, is the time taken for the departure from equilibrium to be reduced to $1/e$th of its initial value. The time of relaxation obeys a relation: $\tau = \tau_0 \exp(E/RT)$, where τ_0 is a constant, E is the activation energy required for the interchange of atomic positions. Introducing the heating or cooling rate $\alpha = \pm dT/dt$ (the positive sign denotes heating) in Equation 20, one has:

$$\tau\alpha\frac{d\theta}{dT} \pm \theta = T \quad (21)$$

Solution of Equation 21 can be achieved by obtaining an integration factor, yielding:

$$\theta = \left[\frac{I(T)}{\tau_0\alpha} + \theta_0 \exp\left(\frac{\Omega_0}{\tau_0}\right)\right]\exp\left(-\frac{\Omega}{\tau_0}\right) \quad (22)$$

in which:

$$I(T) = \int_{\theta_0}^{T} T \exp\frac{\Omega(T)}{\tau_0}\exp\left(-\frac{E}{RT}\right)dT,$$

where θ_0, which determines the final metastable state of the alloy, can be estimated accordingly to [11]:

$$\frac{E}{R\theta_0} = \ln\left(\frac{R\theta_0^2}{\alpha_c \tau_0 E}\right) \tag{23}$$

α_c being the cooling rate,

$$\Omega = \frac{E}{\alpha R} p(x), \qquad \Omega_0 = \Omega(\theta_0)$$

where

$$p(x) = \int_0^x \frac{\exp(-x)}{x^2} dx$$

$$\simeq (x + 2)^{-1} x^{-1} \exp(-x),$$

and

$$x = \frac{E}{RT}$$

As long as $E\tau_0/RT^2 \gg \exp(-E/RT)$, the approximate solution:

$$\theta = \frac{1}{\tau_0 \alpha} \int_{\theta_0}^{T} T \exp\left(-\frac{E}{RT}\right) dT + \theta_0 \tag{24}$$

can be used. This last integral is tabulated in the literature [12]. From Equation 22 for $\theta = T_c$ one has for the maximum permissible heating rate:

$$\alpha_m = \frac{I(T_c)}{\tau_0} 1 \Big/ \left[T_c \exp\left(\frac{\Omega_c}{\tau_0}\right) - \theta_0 \exp\left(\frac{\Omega_0}{\tau_0}\right) \right] \tag{25}$$

where $\Omega_c = \Omega(T_c)$ and T_c is the critical temperature for a given α. Usually α should be chosen as low as possible, but compatible with an observable trace. If Equation 24 is suitable:

$$\alpha_m = \frac{1}{\tau_0 (T_c - \theta_0)} \int_{\theta_0}^{T_c} T \exp\left(-\frac{E}{RT}\right) dT \tag{26}$$

Equations 25 and 26 require to be solved by an iterative process, since both right side terms are a function of α. If α_m results are higher than the value employed in the experiment, this last value is permissible for performing the DSC run, otherwise a lower value must be chosen. Alternatively, if the DSC run is carried out at some heating rate α, the θ–T path can be calculated, and the temperature at which $\theta = T$ can be determined. If such temperature results are lower than T_c, the value of α is allowed to be used, if not, the experience should be again repeated with a lower α until the above condition is fulfilled.

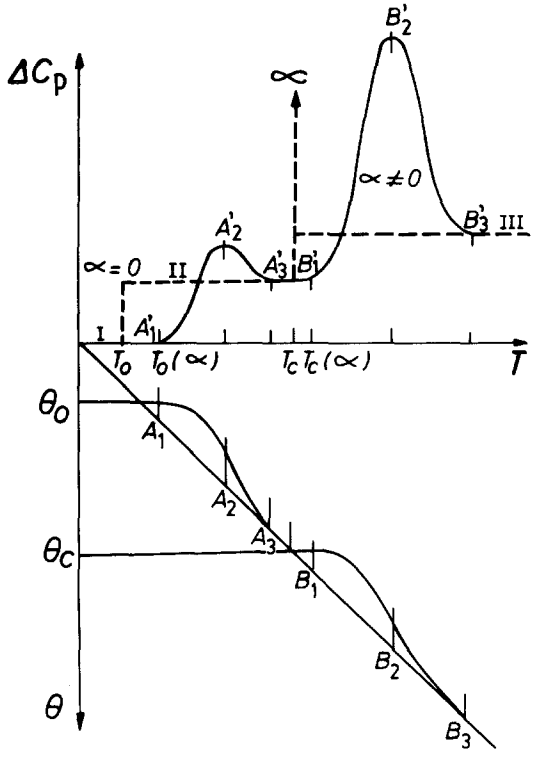

Figure 1 Schematic representation of the interdependence between DSC thermograms and θ–T paths. (Explanation of details is given in the text.)

It is noteworthy to compare schematically the interdependence between θ–T plots and DSC thermograms when a transition from the frozen state followed by dissolution takes place. Fig. 1 shows such a dependence when $\alpha < \alpha_m$ is satisfied. If $\alpha \to 0$, the transition from I to II occurs simply at $T = T_0$; the base line jumps discontinuously to region II. For $\alpha < \alpha_m$, the onset temperature at which the DSC trace leaves region I coincides with that of the θ–T diagram for which $d\theta/dT$ is no longer zero ($A_1A'_1$). The peak temperature of the transition, characteristic of the maximum reaction rate, corresponds to the inflection point on the θ–T plot and so the rate of approach to equilibrium becomes a maximum at that temperature determined by the condition $(d^2\theta/dT^2) = 0$ ($A_2A'_2$). Finally, dynamic equilibrium is achieved at the temperature at which the new base line is reached on the trace, reflected on the θ–T diagram by the threshold temperature for which $(d\theta/dT) = 1$ (AA'). As we are concerned with dissolution by

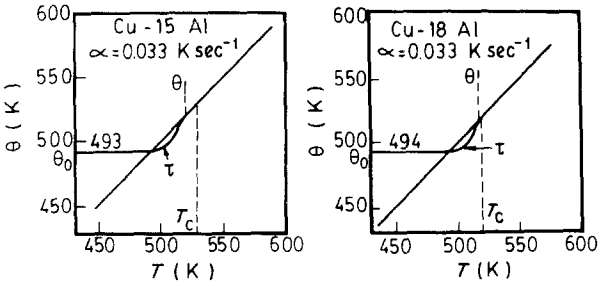

Figure 2 θ–T relation for two alloys furnace cooled at a rate of 15 K h^{-1}. The condition $\theta = T < T_c$ for dynamic equilibrium is achieved in both cases at the indicated heating rate.

a first order transition the differential heat capacity, $\Delta C_p \rightarrow \infty$ if $\alpha \rightarrow 0$ and the transition occurs at the true critical temperature, T_c. For the heating rate considered, T_c shifts to the right, so a somewhat overestimated value for T_c is obtained ($B_1 B'_1$). In fact, for determining the exact value, several runs at different α must be carried out and the different values of T_c should be extrapolated to $\alpha = 0$ in a $T_c(\alpha)$–α plot. However, if $\alpha < \alpha_m$ is small enough, the corresponding overestimate also shifts. The remaining explanation of the scheme of Fig. 1 is straightforward.

3. Results and discussion

All the above analysis will be applied in this section in computing specific interfacial energies of disperse ordered domains in αCu–Al alloys from dissolution DSC traces. Three alloys containing 19/13/6.5 at % Al were furnace cooled at a cooling rate of 15 K h^{-1}. The preparation of these alloys and the details of the microcalorimetric experiments can be found elsewhere [13, 14]. A high purity well-annealed copper sample was used as reference material.

In order to determine the appropriate heating rate to be employed in the DSC runs, available data for E and τ_0 are previously needed. With these data θ_0 can be determined. For Cu–15Al [5, 6] and Cu–18Al [6] the transformation for an equilibrium state of order to another state caused by a sudden small jump of temperature was studied by residual resistivity analysis. From these experiments one finds for Cu–15Al: $\tau_0 = 2.06 \times 10^{-13}$ sec, $E = 151$ kJ mol^{-1} and for Cu–18Al: $\tau_0 = 3.49 \times 10^{-13}$ sec, $E = 181$ kJ mol^{-1}. By substituting each pair of values in Equation 23 and after taking $\alpha_c = 15$ K h^{-1}: $\theta_0 = 493$ and 494 K for Cu–15Al and Cu–18Al, respectively. These values are expected to be almost the same for Cu–13Al and Cu–19Al. Also τ_0 and E for Cu–15Al and Cu–18Al can be assumed to be very close to those for Cu–13Al and Cu–19Al, respectively, because of the low Al content difference between the alloys in each case.

With the computed values of θ_0, τ_0 and E, the θ–T path was calculated for both alloys by means of Equation 22 using tentatively a heating rate $\alpha = 0.033$ K sec^{-1}. The results are plotted in Fig. 2. The critical temperature was determined from the corresponding processed thermograms appearing in Fig. 3 for this heating rate, where the freezing temperature, T_0, is also shown. It can be noticed that the condition $\theta = T$ is reached in both cases at $T < T_c$, ensuring then that the alloys are in dynamic equilibrium at T_c^-. Therefore the value of α selected is appropriate and the enthalpy associated with those thermograms represents ΔH_c. In computing this enthalpy, after each run, the data were converted to plots of differential heat capacity against temperature, using a previously established calibration for the DSC cell. Subsequently, a linear base line was substracted from the data for each alloy. This base line represents the temperature dependent heat capacity of the copper–aluminium solid solutions and the existing ordered domains, and its value was in agreement with the Kopp–Neumann rule. The remainder, the differential heat capacity, ΔC_p, represents the heat associated with the dissolution reaction. The area of the reaction peak in the ΔC_p–T curves between the critical and final temperatures characterizes ΔH_c. The above data reduction procedure has been previously described in the literature [15, 16].

For $\alpha = 0.033$ K sec^{-1}, dynamic equilibrium can be achieved at $T < T_c$ and since a dissolution peak is displayed on the DSC traces for such α, a finite volume fraction exists at T_c^-, and hence the precipitates dissolve by a first order transformation. This result is extended also to Cu–6.5Al.

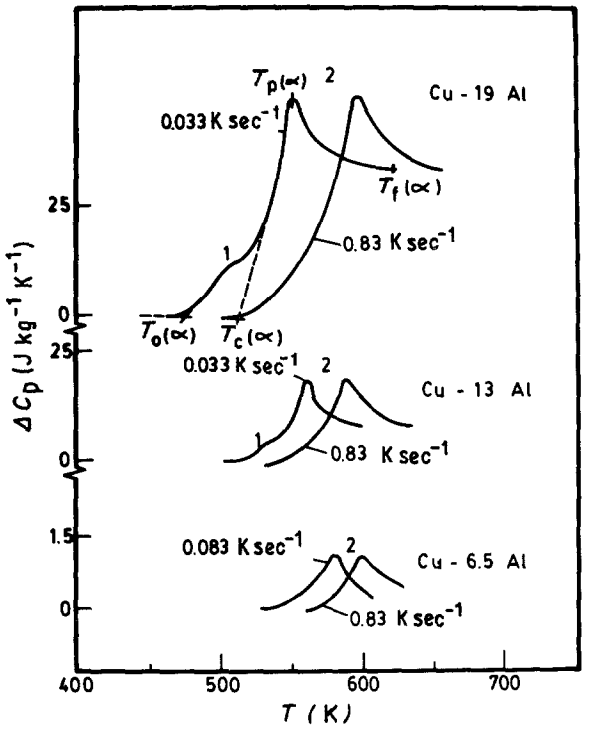

Figure 3 DSC thermograms for αCu–Al alloys furnace cooled at a rate of 15 K h^{-1}. Region II: volume fraction equilibration. Region III: disperse order domain dissolution.

Before computing σ from Equation 11, values V_c and D_c are required. For these alloys $\Delta H_p = 412\,\text{J mol}^{-1}$ [13], $MW_p = 55.2\,\text{kg mol}^{-1}$, $\varrho_p = 7.22 \times 10^3\,\text{kg m}^{-3}$ and $\varrho_s = 8.3 \times 10^3/8.5 \times 10^3/8.7 \times 10^3\,\text{kg m}^{-3}$ for 19/13/6.5Al. With the above data, V_c can be computed by means of Equation 19. D_0 and N were measured electron microscopically at room temperature [7]. The values obtained for D_0 were 20 and 10 nm for alloys containing 15 and 10 at % Al, respectively, while $N = 6 \times 10^{22}\,\text{m}^{-3}$ was the same for both Al concentrations. On the other hand, the enthalpy associated with the thermograms of Fig. 2 corresponding to $\alpha = 0.83\,\text{K sec}^{-1}$ gives ΔH_0, which represents essentially the dissolution energy of the precipitate volume fraction prevailing at room temperature. It can easily be shown in θ–T plots constructed with $\alpha = 0.83\,\text{K sec}^{-1}$, that the condition $\theta = T$ is always reached far above the fictitious critical temperature determined for this value of α. Hence by means of Equations 2 and 17, considering that $V_0 \propto \Delta H_0$, values for D_c can be estimated. All the above data are summarized in Table I together with the computed values for σ obtained for Equation 11. (The values of V_m employed. in Equation 11 were determined as set out below*.)

Calculations considering both the chemical and the geometrical contributions to solid state interfaces [4], show that typical values in the range of 10 to 200 mJ m^{-2} are characteristic for coherent interfaces where there are no geometrical contributions and 100 to 1000 mJ m^{-2} for semi-coherent and non-coherent interfaces. Therefore, it is expected that ordered domains are fully coherent for alloys containing up to 13 to 14 at % Al, while for alloys containing more than 15 at % Al, geometrical contributions must exist. The computed values for σ are in excellent agreement with the experimental predictions, since for Cu–18Al, a transition from disperse order characterized by coherent precipitates [5, 6] to a microdomain structure was found [6, 19]. Furthermore, if the transition from coherence to semi-coherence is analysed in terms of the computed values of D_c, the results are also in agreement with those expected via σ. In so doing, it is necessary to estimate D_{cr}, the critical diameter at which perfect coherence breakdown takes place.

*The molar volume V_m of the ordered domains is based on the stoichiometric Cu_3Al "molecule". Since there is one molecule/unit cell, $V_m = N_0 d^3$, where N_0 is the Avogadro number and d is the lattice parameter of the unit cell, 0.37 m. This value was determined from Vegard's law as a first approximation. $V_m = 30.75 \times 10^{-6}\,\text{m}^3\,\text{mol}^{-1}$. A value for $c_p = 0.228$ was employed [17].

TABLE I Particle–matrix specific interfacial energies for αCu–Al alloys

at % Al	T_c (K)	D_0 (nm)	D_c (nm)	ΔH_0 (J mol^{-1})	ΔH_c (J mol^{-1})	V_0	V_c	$\sigma^{\ddagger}$ (mJ m^{-2})
19	522	27	24	266	164	0.55	0.4	498 ± 19
15	511*	20*	17.2	93†	75†	0.23	0.18	253 ± 8
13	537	16.2	13.6	50	19.3	0.12	0.07	93 ± 4
10	536*	10*	9.4	12†	9.0†	0.03	0.022	30 ± 1.5
6.5	543	7.8	5.8	5.8	4.3	0.015	0.01	16 ± 1

*From [18].
†Interpolated values.
‡Average values computed from five DSC runs.

According to the simple criterion by Brooks [20], D_{cr} is related to the length of the interface required to build a misfit equal to the Burgers vector $\boldsymbol{b}(=0.26\,\text{nm})$ of an interface dislocation. It can be expressed as:

$$D_{cr} = \frac{3\boldsymbol{b}}{\delta}, \tag{27}$$

whereby δ is the atomic volume misfit. On the copper-rich side of Cu–Al, δ is of the order of 0.051 [21]: $D_{cr} = 15.4\,\text{nm}$, thus indicating that full coherence breakdown at a composition somewhat lower than 15Al, as predicted by the former arguments. Therefore, the use of Equation 27 in conjunction with Equations 11 or 14 allow one to estimate the limiting specific interfacial enthalpy for a particular dispersed phase associated to the loss of coherence with the matrix.

The method developed here to measure σ is, in principle, applicable also to particles dissolving by a first order transformation but undergoing coarsening. In this case an equilibrium particle diameter at each temperature does not exist (precipitate size becomes system history dependent), hence volume fraction equilibration via particle size adjustment is not possible as in the previous situation. Furthermore, dynamic equilibration through simultaneous coarsening and change in particle number is not likely to be reached below T_c, since the DSC dynamic experiment is too rapid, even at low heating rates, to be able to monitor the coarsening rate. Therefore, if Equations 11 or 14 are applied for computing σ, making use of non-isothermal calorimetric data, V_c (from Equation 19) and D_c (from Equation 17 or 18) have no longer their assigned meanings but essentially they represent the volume fraction and average particle diameter existing after an anneal at a given temperature during a certain time. (A characteristic feature is the time invariance of the volume fraction of the disperse phase during coarsening; in principle, there is a small increase due to the dependence of the equilibrium solubility on particle size, but this is considered negligible compared with the increase that occurs during precipitation.) Since that volume fraction is generally larger than the equilibrium value expected at T_c^-, the corresponding dissolution enthalpy measured from the DSC trace should also be larger than ΔH_c and consequently, the computed value of σ for the measured precipitate diameter may result in a somewhat overestimated value. More reliable values for σ can be obtained if before the non-isothermal run is carried out, the alloy is annealed at a temperature as close as possible to T_c for different times in order to obtain different degrees of coarsening. The former analysis indicates the incidence of particle diameters on σ, which are not revealed, in general, from determination based upon isothermal coarsening kinetic experiments [22].

Other alloy systems for which particle specific surface enthalpy can be eventually determined on the grounds above, are those containing metastable precipitates against ripening. Metastability can be achieved by interaction energy effects between particles [23–25]. Since in these alloys stable linear arrays of precipitates elastically locked are formed, impingement should be absent even at larger volume fractions. In this case, V_{ex} (Equation 3) instead of V (Equation 2) must be substituted into Equation 5 before the procedures reported here are undertaken, in order to evaluate σ. If one designates the specific surface enthalpy for these microstructural stable arrays as σ_{ex}, it is easy to demonstrate that:

$$\sigma_{ex} = \frac{\sigma_f}{1 - V_c} = \sigma\,[V_c/(1 - V_c)] \times \left[1/\ln\left(\frac{1}{1 - V_c}\right)\right]$$

However, to date, no experiments reporting the order of the transformation associated to the dissolution process are available for such arrays and hence, it is not worth considering this case in more detail at the present time.

In closing, it is notable that in a first order transformation, two phases can coexist in thermodynamic equilibrium at a temperature T_c, having usually different specific volumes at T_c. In a solid material, this volume discontinuity must be accommodated either by elastic strains producing elastic stresses if the crystal lattices remain coherent across the interface, or by plastic deformation if the induced stresses are greater than the elastic limit [26]. The elastic strains can change the behaviour of the critical effects and even the nature of the transition [27]. Although these facts have been disregarded in this simplified approach, it still provides an easy and rapid method to estimate the specific interfacial energy for precipitates or ordered domains dissolving by a first order transformation.

Appendix

The rate of variation of c_M and D with temperature may be obtained from Equations 6 and 7. By evaluating the partial derivatives there involved we have:

$$\frac{\partial c_M}{\partial T} = \frac{12V_m(\bar{c} - Vc_p)(c_p - \bar{c}) \ln [1/(1 - V)]}{TJ} \quad (A1)$$

and

$$\frac{\partial D}{\partial T} = -\frac{4V_m(\bar{c} - Vc_p)(1 - V)D}{(c_p - \bar{c})TJ} \quad (A2)$$

where

$$J = 3DRT(c_p - \bar{c}) \ln [1/(1 - V)] - (\bar{c} - Vc_p)4V_m\sigma. \quad (A3)$$

After imposing the boundary conditions:

$$D = 0, V = 0 \text{ for } T = T_c^+$$

and

$$J = 0 \text{ for } T = T_c^-$$

it follows that:

$$\frac{\partial c_M}{\partial T} > 0 \text{ for } T < T_c;$$

$$\frac{\partial c_M}{\partial T} = 0, c_M = \bar{c} \text{ for } T > T_c$$

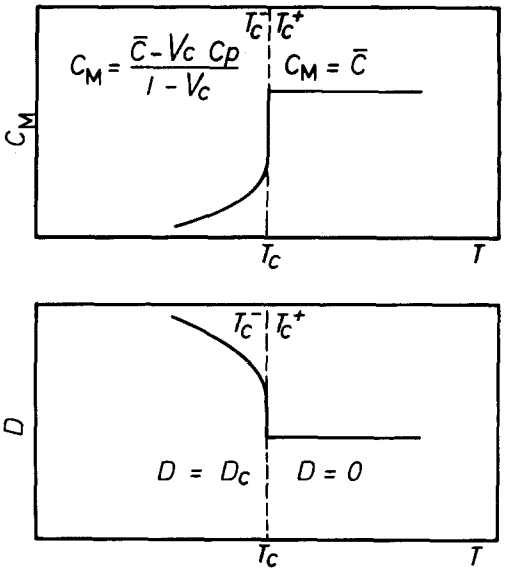

Figure A1 Schematic illustration of the dependence of c_M and D upon T under equilibrium conditions.

and

$$\frac{\partial D}{\partial T} < 0 \text{ for } T < T_c;$$

$$\frac{\partial D}{\partial T} = 0, D = 0 \text{ for } T > T_c$$

as required. The functional dependence of c_M and D with temperature is shown schematically in Fig. A1.

Acknowledgements

The author wishes to thank the Departmento de Investigación y Bibliotecas de la Universidad de Chile for financial support under Contract I-2294-8515 and to the Instituto de Investigaciones y Ensayes de Materiales, Facultad de Ciencias Fisicas y Matemáticas, Universidad de Chile also for financial support and for the facilities given for this research.

References

1. R. C. GIFKINS (Ed.), "Interfaces" (Butterworths, Sevenoaks, Kent, UK, 1969).
2. E. D. HONDROS, *ibid.*, p. 77.
3. J. J. KRAMER, G. M. POUND and R. F. MEHI, *Acta. Metall.* **6** (1958) 763.
4. J. D. BOYD and R. B. NICHOLSON, *ibid.* **9** (1971) 1101.
5. G. VEITH, L. TRIEB, W. PUSCHL and H. P. AUBAUER, *Phys. Status. Solidi* **27** (1975) 59.
6. L. TRIEB and G. VEITH, *Acta. Metall.* **26** (1978) 185.

7. W. GAUDIG and H. WARLIMONT, *Z. Metallkde.* **60** (1969) 488.
8. C. A. JOHNSON, *Surf. Sci.* **3** (1965) 429.
9. M. AVRAMI, *J. Chem. Phys.* **7** (1939) 1103.
10. J. D. VERHOEVEN, "Fundamentals of Physical Metallurgy" (John Wiley, New York, 1974) p. 401.
11. E. W. BRAGG and E. J. WILLIAMS, *Proc. Roy. Soc.* **145A** (1934) 699.
12. J. E. HOUSE Jr and J. D. HOUSE, *Thermochim. Acta* **54** (1982) 213.
13. A. VARSCHAVSKY, *Met. Trans.* **13A** (1982) 801.
14. A. VARSCHAVSKY and E. DONOSO, *ibid.* **14A** (1983) 875.
15. R. DELASI and P. N. ADLER, *ibid.* **8A** (1977) 1177.
16. J. M. PAPAZIAN, *ibid.* **13A** (1982) 761.
17. M. SEHETBAUER, L. TRIEB and M. P. AUBAUER, *Z. Metallkde* **67** (1976) 431.
18. S. MATSUO and L. M. CLARENBROUGH, *Acta. Metall.* **29** (1963) 709.
19. W. GAUDIG and H. WARLIMONT, *ibid.* **29** (1978) 709.
20. H. BROOKS, "Metal Interfaces" (American Society for Metals, Cleveland, Ohio, 1952) p. 20.
21. H. W. KING, *J. Mater. Sci.* **1** (1966) 79.
22. J. M. MADER, A. H. HEUER and T. E. MITCHELL, "Solid-Solid Phase Transformations", edited by H. I. Aaronson, D. E. Laughlin, R. F. Sekerka and C. M. Wayman, (The Metallurgical Society of AIME, Warrendale, Pennsylvania, 1982) p. 727.
23. W. M. STOBBS and G. R. PURDY, *Acta. Metall.* **26** (1978) 1069.
24. V. PEROVIC, G. R. PURDY and L. M. BROWN, *ibid.* **21** (1979) 1075.
25. *Idem, ibid.* **29** (1981) 889.
26. V. RAGHRARAN and M. COHEN, "Treatise on Solid State Chemistry", Vol. 5, edited by M. B. Hanay, (Plenum Press, New York, 1975) p. 67.
27. P. J. BERGMAN and B. J. HALPERIN, *Phys. Rev.* **13B** (1976) 2145.

Received 11 May
and accepted 15 October 1984